SCIENTIFIC REPORTS

OPEN

SUBJECT AREAS:
PLASMA PHYSICS
APPLIED PHYSICS

Received
7 May 2014

Accepted
20 August 2014

Published
10 September 2014

Correspondence and requests for materials should be addressed to J.T. (tangjie1979@opt.ac.cn)

Characterization of argon direct-current glow discharge with a longitudinal electric field applied at ambient air

Weiman Jiang[1], Jie Tang[1], Yishan Wang[1], Wei Zhao[1] & Yixiang Duan[1,2]

[1]State Key Laboratory of Transient Optics and Photonics, Xi'an Institute of Optics and Precision Mechanics of CAS, Xi'an 710119, China, [2]Research Center of Analytical Instrumentation, Sichuan University, Chengdu 610064, China.

A direct-current-driven plasma jet is developed by applying a longitudinal electric field on the flowing argon at ambient air. This plasma shows a torch shape with its cross-section increased from the anode to the cathode. Comparison with its counterparts indicates that the gas flow plays a key role in variation of the plasma structure and contributes much to enlarging the plasma volume. It is also found that the circular hollow metal base promotes generation of plasma with a high-power volume density in a limited space. The optical emission spectroscopy (OES) diagnosis indicates that the plasma comprises many reactive species, such as OH, O, excited N_2, and Ar metastables. Examination of the rotational and vibrational temperature indicates that the plasma is under nonequilibrium condition and the excited species OH($A\ ^2\Sigma^+$), O(^{5}P), and N_2($C\ ^3\Pi_u$) are partly generated by energy transfer from argon metastables. The spatially resolved OES of plasma reveals that the negative glow, Faraday dark space, and positive column are distributed across the gas gap. The absence of the anode glow is attributed to the fact that many electrons in the vicinity of the anode follow ions into the positive column due to the ambipolar diffusion in the flowing gas.

Atmospheric pressure nonequilibrium plasmas recently have attracted a great interest largely because it can be used for a wide range of applications, such as surface modification, thin film deposition, and biological decontamination, without the need for an expensive vacuum system[1–4]. Such plasmas are usually produced by different kinds of discharges like corona, capillary, direct-current (DC), radio frequency, microwave, and dielectric-barrier discharges[5]. DC glow discharge is a popular one among them, with the voltage applied between two naked electrodes. The DC glow discharge was first observed with helium, neon, and nitrogen used as working gas in a tube at the low pressure, and characterized by different regions depending on the discharge parameters (e.g., the geometry of the electrodes, the gas type, and the pressure)[6]. This kind of discharge was also successfully generated at high pressure, even at atmospheric pressure in the ambient air, though there exist undesirable instabilities which lead a glow to arc transition. Different geometries of electrode and different types of gas were employed to characterize the DC glow discharge in laboratory. A DC microhollow cathode discharge (MHCD) in atmospheric pressure air has been reported by Stark and Schoenbach[7–8]. The stability of this plasma is attributed to the fact that the microhollow cathode supplies electrons to the positive column of the discharge rather than the instability prone cathode region as in a traditional glow discharge. Another DC glow discharge was generated between a thin cylindrical anode and a flat cathode with helium, argon, hydrogen, nitrogen and air used as working gas respectively[9]. The discharges appeared to operate as temperature and pressure scaled versions of low pressure discharges. It is possible to distinguish negative glow, Faraday dark space, and positive column regions of the discharge in the normal glow discharges. Investigations of atmospheric pressure glow discharges in helium, argon, nitrogen and air in the similar electrode configuration were presented[10]. Experiment results showed that for all the gases, plasma non-equilibrium degree in a positive column decreases with discharge current increase.

It is generally accepted that a high speed gas flow is beneficial to improvement of discharge stabilities due to sufficient cooling of discharges at high pressures. A stable brush-shaped plasma jet was achieved by introducing a flowing argon through the narrow slit with two cylindrical electrodes set opposite at its ends and powered by a DC supply[11]. Here, a transverse electric field was applied on the flowing gas with its flow direction perpendicular to the field. The spatially resolved optical emission spectroscopy (OES) of the plasma revealed that the negative glow, positive column, and anode glow exist across the gas gap. Li *et al.* employed the similar device as that used in Ref. 11 to generate a brush-shaped plasma jet[12], where the same spatial discharge structure was observed. Another

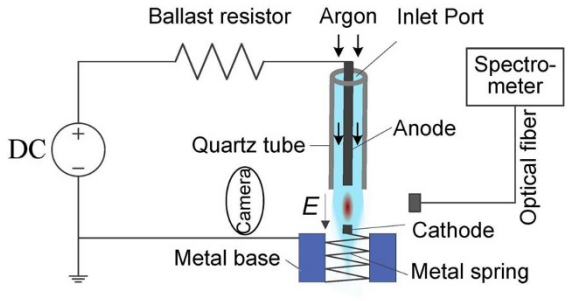

Figure 1 | **The experimental setup.**

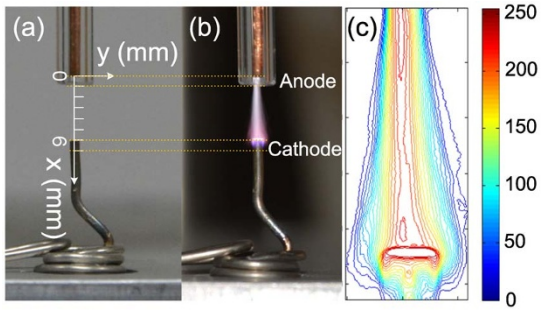

Figure 3 | Photographs of (a) the experimental apparatus and (b) the plasma jet generated between two rod electrodes with the electrode spacing of 6 mm (with the exposure time of 20 ms).(c) shows the isointensity map of the plasma image out of the quartz tube.

electrode configuration was reported by Lu *et al.*[13]. A high-voltage pulsed DC power supply was connected to the blades that serve as the anode and the treated objects were connected to the ground, where a longitudinal electric field was applied on the flowing gas. The negative glow, Faraday dark space and positive column in the brush-shaped plasma are clearly visible to the naked eye. Additionally, a DC-driven plasma source equipped with hollow-needle-plate electrodes was developed by Li *et al.*[14], where the gas flows along the cavity of the hollow needle and rushes to the plate. This plasma presents us a diffuse plume in cup shape in the discharge space. As mentioned above, in order to obtain a stable plasma, the working gas was allowed to flow through the discharge space with either a transverse or a longitudinal electric field applied on. As for the longitudinal electric field, the working gas flows from one electrode to the other, where the needle-plate (or rod-plate) electrodes are usually used. In this work, a plasma jet is generated by using a longitudinal electric field that is generated between two rod electrodes. This plasma shows quite different physical structure in comparison with those observed in the traditional DC glow discharge.

Results

To demonstrate the unique DC-driven plasma jet, we used the atmospheric-pressure plasma device sketched in Fig. 1. The voltage-current (V-I) characteristic of the DC discharge was examined at the gas flow 2 L/min, with the relationship between the discharge voltage and current shown in Fig. 2. It is found that only subnormal (zone I) and normal (zone II) glow discharge modes appear in the examined current scope of 9–33 mA, where the Townsend mode is not observed. In the subnormal glow discharge (9–18 mA), the V–I curve assumes a negative differential resistance and the discharge voltage across the gas gap drops with the increasing current. When the discharge is transformed to the normal one (18–33 mA), the V–I curve becomes essentially flat and the discharge voltage approximately maintains a constant with the increasing current.

Figure 3(a) shows the experimental apparatus without discharge. When the apparatus works at an operating point with the discharge voltage of 234 V and current of 22 mA, the discharge operates in the normal glow mode and a stable plasma jet is formed between the two electrodes, as shown in Fig. 3(b). The plasma photograph was taken by using a digital camera (Nikon D5200) with the exposure time of 20 ms. The plasma appears to eject out of the quartz tube from the end face of the anode and run towards the cathode, and gradually becomes thick from the top to the bottom, looking like an inverted torch. The diameter of the plasma jet is approximately linearly increased from 1 mm close to the anode to about 3 mm around the cathode, exhibiting an increasing cross-section. A closer observation indicates that parts of the plasma run out of the discharge space between the electrodes along the gas flow direction and surround the cathode end face. Figure 3(c) shows the isointensity map of the plasma image out of the quartz tube (with x varied from 1 to 7 mm). It is found that the luminance of the plasma is weakened along the radial direction.

To investigate reactive species in the plasma, the OES was examined by using a moderate-resolution spectrometer with its fiber arranged at the specific spot (x = 3 mm and y = 0 mm) in accordance with the axe labeled in Fig. 3. Typical emission spectra with the wavelength range from 200 to 1000 nm are depicted in Fig. 4. In the ultraviolet and visible region, between 200 and 450 nm, the spectra are dominated by $N_2(C\ ^3\Pi_u \rightarrow B\ ^3\Pi_g)$ emissions. Additionally, the OH emission lines, resulted from $OH(A\ ^2\Sigma^+ \rightarrow X\ ^2\Pi)$ transition, are also visible. In the visible and infrared region between 690 and 950 nm, we can easily observe various excited argon atomic lines (e.g., λ = 763.7, 772.7, and 811.7 nm) from the 4 p → 4 s transitions. Meanwhile, a group of oxygen atomic lines around 777.8 nm, which correspond to O(I) triplet state transitions ($O(^5P) \rightarrow O(^5S^0)$), are also observed in close wavelength to one another, but cannot be distinguished due to the resolution limit of the spectrometer.

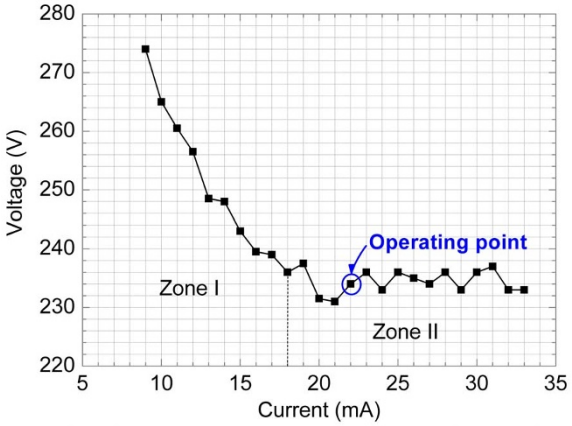

Figure 2 | **Voltage-current characteristic of the plasma source with 2 L/min argon as working gas at atmospheric pressure.**

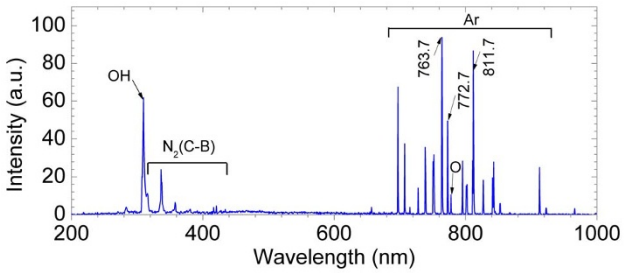

Figure 4 | **The emission spectrum of the plasma jet examined at the spot with x = 3 mm and y = 0 mm.**

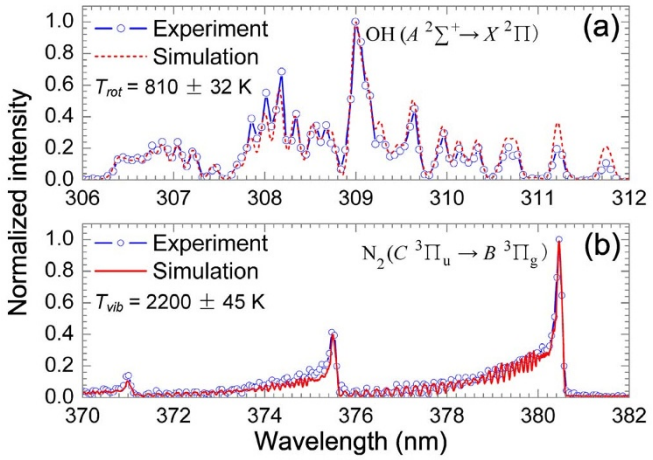

Figure 5 | The comparison of experimental and simulated spectra of (a) OH($A\ ^2\Sigma^+ \rightarrow X\ ^2\Pi$, $\Delta v = 0$) transition for T_{rot} measurement and (b) $N_2(C\ ^3\Pi_u \rightarrow B\ ^3\Pi_g$, $\Delta v = -2$) transition for T_{vib} measurement.

Due to frequent collisions among heavy particles at atmospheric pressure, the rotational temperature (T_{rot}) of the OH radical has a value which is generally close to the gas temperature[15,16]. This temperature can be measured by using the OH($A\ ^2\Sigma^+ \rightarrow X\ ^2\Pi$, $\Delta v = 0$) band transition from 306 to 312 nm. This band is easily isolated under various experimental conditions to give useful information. The vibrational temperature (T_{vib}) provides the information of the energy transfer between electrons and heavy particles, especially molecules[17]. It was obtained by the typical Boltzmann plot method of the nitrogen second positive system $N_2(C\ ^3\Pi_u \rightarrow B\ ^3\Pi_g, \Delta v = -2)$ in the range 370–382 nm[18]. Based on the emission spectrum measured by using the high-resolution spectrometer with the fiber probe arranged at the same spot (x = 3 mm and y = 0 mm), the rotational temperature and vibrational temperature of the plasma were obtained through the analysis of OH and N_2 molecular emission spectrum, respectively. As seen from Fig. 5, the simulated spectra at T_{rot} = 810 ± 32 K and T_{vib} = 2200 ± 45 K give a good fit to the experimental spectra, indicating that the vibrational temperature is higher than the rotational temperature.

The spatially resolved OES of reactive species such as OH (309.7 nm), N_2 (337.1 nm), and Ar (763.7 nm) was examined along the x axis or axial direction at y = 0 mm (from the anode to the cathode labeled in Fig. 3), with the result shown in Fig. 6(a), where the discharge current is 22 mA. It is found that the OH and Ar assume the similar spatial distribution of emission profile. Their OES intensity first increases along the x axis (0–1 mm), and then approximately maintains unvaried (1–4 mm). After a slight drop (4–5 mm), the intensity rises largely, reaches its maximum around x = 6 mm, afterwards gradually declines, and tends to be zero near the cathode (6–7 mm). This spatial distribution feature of OES indirectly reveals that the negative glow (around x = 6 mm), Faraday dark space (around x = 5 mm), and positive column (1–4 mm) are distributed from the cathode to the anode. The OES intensity of N_2 exhibits a quite different spatial distribution, in comparison with that of OH and Ar. Its intensity maintains very low and nearly unvaried from x = 0 to 3 mm. After a slow increase (3–5 mm), the intensity rises sharply (5–6 mm), approaches its maximum around 6 mm, and drops rapidly near the cathode (6–7 mm).

Figure 6(b) shows the OES spatial distribution of a stable brush-shaped plasma jet generated in an extended DC discharge by applying a transverse electric field on the flowing argon, which was presented in our previous work[11]. This DC discharge was supported by a DBD one and operated in a normal glow mode at discharge current 22 mA. The OES of the plasma was examined along the x axis (from the cathode to the anode) with the distance 2 mm away from the exit.

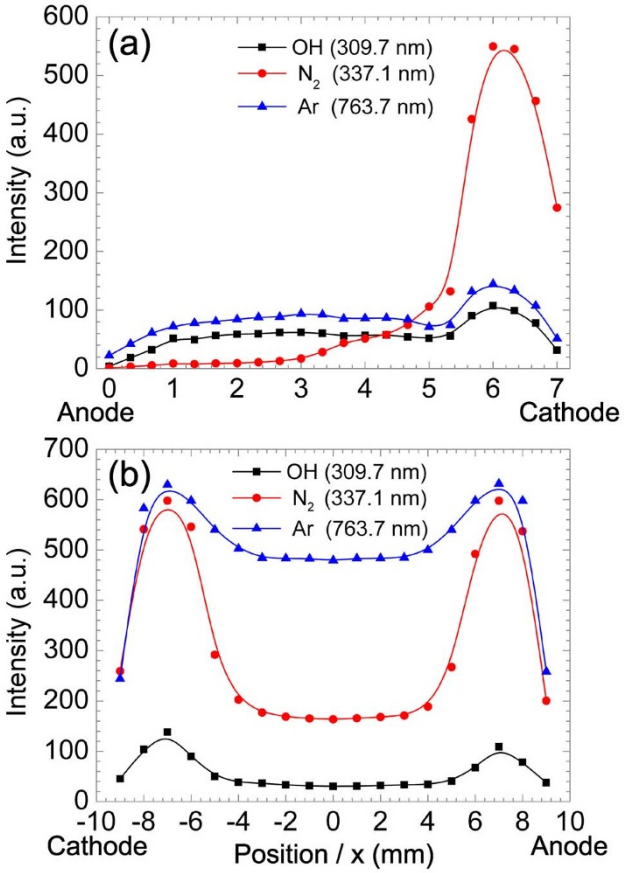

Figure 6 | Emission profiles of the radical OH (309.7 nm), excited N_2 (337.1 nm), and excited argon (763.7 nm) along x axis with a longitudinal (a) and transverse (b) electric field applied on the flowing gas, respectively.

The spatially resolved OES showed that all of these reactive species presented a near-symmetrical distribution of emission profile, with the greatest emission intensity at the edges.

The spatially resolved OES of these reactive species was also examined along the y axis with x = 3 and 6 mm labeled in Fig. 3. Figure 7 shows that the emission intensity of all the reactive species presents a symmetric distribution with its maximum at the center. Along the y direction at x = 3 mm, the light emitted from the excited argon exceeds that from other species and the N_2 exhibits the weakest emission intensity, as shown in Fig. 7 (a). With x = 6 mm, as seen from Fig. 7 (b), the light emitted from excited N_2 is relatively increased considerably and overwhelms both other species of light along the y axis. The OH emission intensity becomes the weakest one.

The spatial distribution of rotational and vibrational temperature was measured through the spectral fitting method along the x axis at y = 0 mm, with the results depicted in Fig. 8. The errors in the measured rotational and vibrational temperature are less than ±40 and ±50 K, respectively. As seen from Fig. 8 (a), the highest rotational temperature (1050 K) is located in the negative glow region and there is a decrease of temperature close to the Faraday dark space. After the Faraday dark space, this temperature rises gradually and approaches about 810 K in the positive column. Approaching the anode, the temperature decreases to about 630 K. Figure 8 (b) shows a distinct increase of vibrational temperature from the negative glow region to the Faraday dark space where the temperature arrives at its maximum of 2450 K. This temperature reduces after the Faraday dark space and reaches about 2200 K in the positive column. The measured rotational and vibrational temperature profiles are in well agreement with those reported by Staack *et al.*[19].

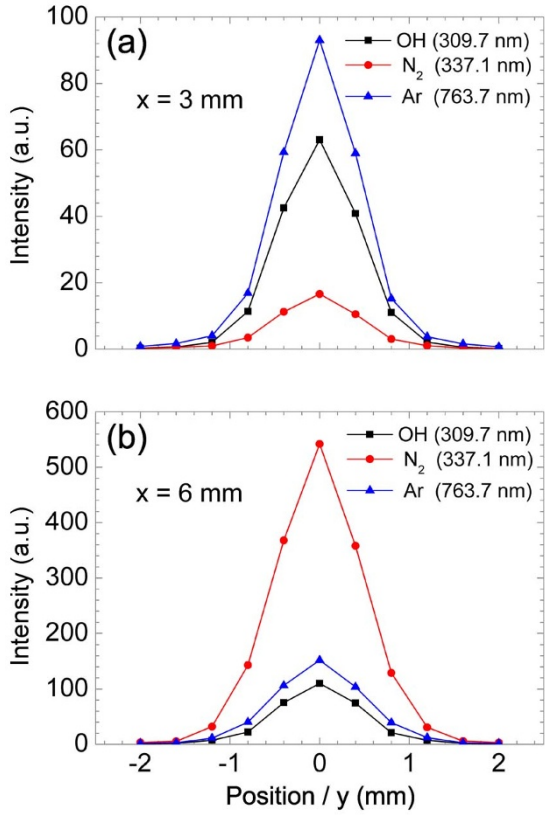

Figure 7 | Emission profiles of the radical OH (309.7 nm), excited N_2 (337.1 nm), and excited argon (763.7 nm) along the y axis with x fixed at (a) 3 mm and (b) 6 mm, respectively.

Discussion

In the traditional DC normal glow discharge in a still argon at atmospheric pressure, the contraction of the positive column, which is attributed to the recombination process, allows the gas discharge to occur only in the discharge space between two opposite plane electrodes[6,20]. The cross-section of the positive column has been changed little along the axial direction (from the anode to the cathode)[10]. Comparison with the torch-shaped plasma jet in our case (see Fig. 3(b)) indicates that the gas flow plays a key role in variation of the plasma structure and contributes much to enlarging the plasma volume along the radial direction especially in the vicinity of the cathode. In the work performed by Li *et al.*[14], a cup-shaped plasma could be formed between the hollow-needle anode and the plate cathode. The backflow gas and the large-area plate cathode are responsible for the large-volume diffuse plasma generated in the vicinity of the cathode. In our case, the circular hollow metal base avoids the gas backflow and gas dispersion to a larger open space around the discharge region. This promotes the formation of a thin gas flow channel around the column of the discharge region, leading to the generation of plasma with a high-power volume density in a limited space. This feature is crucial in applications such as surface modification, where a high-power-density plasma is required.

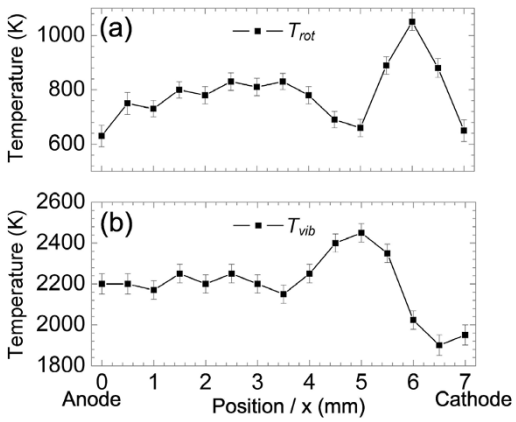

Figure 8 | The spatial distributions of (a) rotational temperature and (b) vibrational temperature along the x axis at y = 0 mm.

As we know, reactive species, such as OH and O, are the indispensable components and main enablers for industrial and medical plasma treatment applications. The OES of the torch-shaped plasma jet indicates that many reactive species, including OH, O, excited N_2, and argon metastables, are produced in the glow discharge, as shown in Fig. 4. All these reactive species are desirable in the applications such as surface modification and biological decontamination. Since the plasma jet is generated in the ambient air, the presence of OH, O and excited N_2 spectra is attributed to the interaction of the argon plasma with the ambient air that contains nitrogen, oxygen, water vapor, and other components, which will be addressed in detail in the following section.

Examination of the rotational temperature and vibrational temperature of the plasma in Fig. 5 shows that the plasma jet is under nonequilibrium condition. This feature is favorable for enhanced plasma chemistry. The electronic excitation temperature T_{exc} of plasma is determined according to the double-line method[21]:

$$T_{exc} = \frac{\alpha|\xi_1 - \xi_2|}{\lg\frac{g_1A_1}{g_2A_2} - \lg\frac{\lambda_1}{\lambda_2} - \lg\frac{i_1}{i_2}}, \quad (1)$$

where two close spectral lines (λ_1 = 763.7 nm, $2P_6 \rightarrow 1S_5$, and λ_2 = 772.7 nm, $2P_2 \rightarrow 1S_3$) are used; excitation potentials of the spectral lines ξ_1 = 13.17 eV and ξ_2 = 13.328 eV; the coefficient α is 5040 for ξ in eV; the weighting factor $g_1 = 5$ and $g_2 = 3$; transition probability of the two spectral lines A_1 = 24.5 and A_2 = 11.7; and i is the relative intensity of spectral line with $i_1 \approx 45800$ and $i_2 \approx 17100$[22], The electronic excitation temperature is estimated to be 0.57 ± 0.02 eV (6586 ± 240 K) and far beyond the vibrational temperature. This also indicates the nonequilibrium characteristic of the plasma jet.

However, the vibrational temperature determined through analysis of N_2 emission spectra as a result of electron impact excitation is usually measured to be about 3000 K[23], and much higher than the temperature examined in our case. This suggests that the excited species OH($A\ ^2\Sigma^+$), O(^{5}P), and $N_2(C\ ^3\Pi_u)$ are partly generated by energy transfer from argon metastables, in addition to the electron excitation. As is well known, the energy carried by the argon metastables (11.5–13.5 eV)[24], which are produced effectively in our case indicated by the spectrum shown in Fig. 4, is slightly higher than that of energy level of $N_2(C\ ^3\Pi_u)$ (~11.1 eV) from the ground state[25]. The argon metastables can easily transfer energy to the ground state nitrogen molecules to generate abundant excited state $N_2(C\ ^3\Pi_u)$ molecules. Besides, the energy required to dissociate H_2C from the ambient air into OH and H, and subsequently excite the ground state OH to the excited state OH($A\ ^2\Sigma^+$) is only 5.1 and 4.2 eV respectively[24]. Sufficient excited state OH($A\ ^2\Sigma^+$) molecules can be produced by energy transfer from argon metastabels. Thus, the emission spectra arising from the excited OH and N_2 are distinctively presented. The energy threshold is 15.9 eV for the production of O(^{5}P) from O_2, and is beyond the energy level of the argon metastables[25]. Therefore, the direct generation of excited O from O_2 through energy transfer with excited argon atoms is ignorable in our case. However, the energy for dissociation of an oxygen molecule to oxygen atoms is 5.58 eV and that required to subsequently produce O(^{5}P) from ground state O is about 10.7 eV[25,26]. Since the two potential levels are in the range of the energy carried by argon metastables, the excited O can be produced from their ground state atoms through

energy transfer processes with excited Ar. As a result, the oxygen emission spectra are observed.

The spatially resolved OES of the plasma in Fig. 6(a) presents the spatial emission spectrum distribution of reactive species. As discussed above, the excited OH and N_2 are produced from water vapor and nitrogen in the ambient air through complex reaction channels. The corresponding reaction coefficients are largely dependent on the reaction conditions, such as reactant concentration and energy required for reaction onset. The distinct spatial distribution of OH and N_2 emission spectra is probable due to the largely different volume percent between water vapor and nitrogen in ambient air and different energy required to pump them from the ground state to an excited one[16]. In our experiment, the argon ejects into the ambient air from the end face of the anode with a certain velocity and mixes with the ambient air. The un-fully mixing partly contributes to the low and slowly increasing intensity of N_2 emission spectra in the positive column. In addition, the gas flow brings parts of the excited N_2 downward and few are left upward in the positive column. This contributes much to assembling most of the excited N_2 in the vicinity of the cathode.

In our previous work, as shown in Fig. 6(b), a near-symmetrical distribution of emission profile of reactive species (radical OH, excited N_2, and excited argon) was presented in front of us, with a flat area located in the middle and two peaks situated at the edges. It is considered that the flat area is correlated with the positive column of the DC glow discharge, while the two peaks at the edges is attributed to the negative and anode glow, where there exist many energetic electrons. In this work, the near-symmetrical distribution of emission profile cannot be found, because the peak of emission intensity appears only near the cathode. The absence of the emission intensity peak near the anode suggests that the anode glow does not exist.

Since the gas flow is fixed at 2 L/min and the inner diameter of quartz tube is 1.7 mm, the gas flow velocity near the anode is estimated to be about 1.7×10^3 cm/s. The electric field in the positive column can be expressed as $E = (V_{dis} - V_n)/D$, with the value of 172 V/cm. Here, V_{dis} is the sustaining voltage (234 V) between the electrodes, V_n is the cathode fall (~165 V) for the iron electrode[6] and D is the length of the positive column (~4 mm). The electron drift velocity is given by $v_e = \mu_e E$. With the electron mobility μ_e of 4.3×10^2 $cm^2/(V \cdot s)$[6], the electron drift velocity is approximately equal to 0.7×10^5 cm/s and far beyond the gas flow velocity. This means the gas flow has practically no direct effect on the motion of electrons. As far as the ion motion is concerned, the ion drift velocity $v_i = \mu_i E \approx 0.3 \times 10^3$ cm/s, where only one sort of ions Ar^+ is considered for simplicity and the ion mobility $\mu_i = 1.9$ $cm^2/(V \cdot s)$[27]. It is found that the gas flow velocity can be comparable with the ion drift one and approximately 6 times higher than the latter. Thus, the gas flow has an appreciable effect on the motion of ions. In our case, both the gas and the ions flow from the anode to the cathode and they drift in the same direction, while the electrons travel in the opposite direction. Due to the higher gas flow, acceleration of ions in the positive column is greatly enhanced, so that overmany ions flux through the cross section of positive column per unit time and drift along the electric field. Subsequently, Ion vacancies are formed in the local discharge space. If these ion vacancies are not occupied in time by new ions, parts of electrons will reverse their drift direction and run after the drifting ions by the electrostatic force due to the regime of ambipolar diffusion[6,28]. Under such conditions, many extra ions in the vicinity of the anode are brought into the positive column by the gas flow. The electrons thus follow the ions there. As a result, the electron density near the anode is substantially reduced and the anode glow is absent, showing us an asymmetrical distribution of emission profile.

The emission profile of the reactive species shown in Fig. 7 reveals that the occurrence of chemical reactions are concentrated in the center part of the plasma and most of the reactive species are produced there. When these reactive species are deexcited, they emit a brighter light, as illustrated in Fig. 3(c).

The spatially resolved rotational and vibrational temperature measurements in Fig. 8 show that the discharge is nonthermal throughout the discharge space. The peak and valley in the profile of rotational temperature are associated with heating of the gas by energetic electrons[6]. The rotational temperature peak in the negative glow region is attributed to the more energetic electrons due to the high electric field there. In the Faraday dark space, the electrons are less energetic with a low electric field, resulting in a falling of temperature. The decrease of rotational temperature close to the anode is probably due to the higher gas flow velocity which is beneficial to cooling the plasma. A correspondence between higher vibrational temperature and lower rotational temperature is observed probably due to the increased vibration-translation relaxation rates at higher gas temperature[19,29].

Methods

A schematic of the experiment setup is shown in Fig. 1. The plasma source mainly comprises two parts. One is the anode unit and the other is the cathode unit. In the anode unit, a cylindrical metal rod (with the diameter of 1 mm) serves as the anode that is centered inside a quartz tube (with the inner diameter of 1.7 mm and outer diameter of 3.3 mm). The metal rod is connected to a high-voltage DC power supply through a 100 MΩ ballast resistor which is used to limit the discharge current. As for the cathode unit, a metal (iron) spring acts as the cathode and is embedded in the hollow cylindrical metal base (with the hollow diameter of 7 mm) that is connected to the ground. It should be noted that the metal spring is fixed tightly in the metal base and could hardly be deformed by the gas flow. The anode unit is set above the cathode one with the electrode spacing of 6 mm. Argon (with the purity of 99.999%), which is controlled by a mass flow controller (fixed at 2 L/min), enters by inlet port, flows through the circular region between the quartz tube and the anode, and rushes out into the discharge space, where argon and ambient air are mixed. The volume fraction of water vapor in ambient air is estimated to be 1.9%, based on the temperature of 25°C and the relative humidity of 60% recorded by a humidity/temperature transmitter. With a proper voltage applied to the two electrodes, a stable plasma jet, indicated by the red pattern, can be formed between them. In our experiment, the gas mixture flows from the anode to the cathode and the flow has the same direction with the electric field. After travelling across the discharge space, the gas mixture will flow along the original direction and into the circular hollow space of the metal base, rather than flow back in the case where needle-plate (or rod-plate) electrodes are used. The flow behavior of argon is indicated by the light blue bar with an arrow downstream. The plasma is imaged with a digital camera (Nikon D5200). The emission spectra from the plasma are recorded by using two different resolution spectrometers. For the large emission spectrum range (200–1000 nm), an Avantes spectrometer (AvaSpec-ULS2048-USB2) with a moderate resolution of 0.8 nm is used to identify various reactive species. In order to obtain the rotational and vibrational temperature of the plasma, another Avantes spectrometer (AvaSpec-ULS2048-3-usb2) with a high resolution of 0.1 nm is used. Both their fiber probes are placed at 1.0 cm away and perpendicular to the plasma. The radius of observation spot of fiber probe is 2.3 mm, with the fiber diameter of 200 μm and the fiber numerical aperture of 0.22.

1. Kanzawa, S., Kogoma, M., Okazaki, S. & Moriwaki, T. Glow plasma treatment at atmospheric pressure for surface modification and film deposition. *Nuclear Inst. Methods Phys. Res.* **37**, 842–845 (1989).
2. Kunhardt, E. E. Generation of large-volume, atmospheric-pressure, nonequilibrium plasmas. *IEEE Trans. Plasma Sci.* **28**, 189–200 (2000).
3. Bormashenko, E., Grynyov, R., Bormashenko, Y. & Drori, E. Cold radiofrequency plasma treatment modifies wettability and germination speed of plant seeds. *Sci. Rep.* **2**, 741; DOI:10.1038/srep00741 (2012).
4. Lu, X., Naidis, G. V., Laroussi, M. & Ostrikov, K. Guided ionization waves: Theory and experiments. *Physics Reports* (2014), http://dx.doi.org/10.1016/j.physrep.2014.02.006.
5. Staack, D., Farouk, B., Gutsol, A. & Fridman, A. Characterization of a dc atmospheric pressure normal glow discharge. *Plasma Sources Sci. Technol.* **14**, 700–711 (2005).
6. Raizer, Y. P. *Gas Discharge Physics,* 2nd ed.(Springer, Berlin, Germany, 1991).
7. Stark, R. H. & Schoenbach, K. H. Direct current glow discharges in atmospheric air. *Appl. Phys. Lett.* **74**, 3770–3772 (1999).
8. Stark, R. H. & Schoenbach, K. H. Direct current high-pressure glow discharges. *J. Appl. Phys.* **85**, 2075–2080 (1999).
9. Staack, D., Farouk, B., Gutsol, A. & Fridman, A. DC normal glow discharges in atmospheric pressure atomic and molecular gases. *Plasma Sources Sci. Technol.* **17**, 025013 (2008).
10. Arkhipenko, V. I., Kirillov, A. A., Safronau, Y. A., Simonchik, L. V. & Zgirouski, S. M. Plasma non-equilibrium of the DC normal glow discharges in atmospheric pressure atomic and molecular gases. *Eur. Phys. J. D* **66**, 252 (2012).

11. Tang, J., Li, S., Zhao, W., Wang, Y. & Duan, Y. Development of a stable dielectric-barrier discharge enhanced laminar plasma jet generated at atmospheric pressure. *Appl. Phys. Lett.* **100**, 253505 (2012).
12. Li, X., Liu, R., Jia, P., Bao, W. & Shang, Y. Self-pulsing discharge of a plasma brush operated in atmospheric-pressure argon. *Europhysics letters* **102**, 55003 (2013).
13. Lu, X., Wu, S., Chu, P. K., Liu, D. & Pan, Y. An atmospheric-pressure plasma brush driven by sub-microsecond voltage pulses. *Plasma Sources Sci. Technol.* **20**, 065009 (2011).
14. Li, X., Di, C., Jia, P. & Bao, W. Characteristics of a Direct Current-driven plasma jet operated in open air. *Appl. Phys. Lett.* **103**, 144107 (2013).
15. Pellerin, S., Cormier, J. M., Richard, F., Musiol, K. & Chapelle, J. A spectroscopic diagnostic method using UV OH band spectrum. *J. Phys. D: Appl. Phys.* **29**, 726–739 (1996).
16. Bruggeman, P. J., Sadeghi, N., Schram, D. C. & Linss, V. Gas temperature determination from rotational lines in non-equilibrium plasmas: a review. *Plasma Sources Sci. Technol.* **23**, 023001 (2014).
17. Moon, S. & Choe, W. A uniform glow discharge plasma source at atmospheric pressure. *Appl. Phys. Lett.* **84**, 188–190 (2004).
18. Bruggeman, P. J., Liu, J., Degroote, J., Kong, M. G., Vierendeels, J. & Leys, C. Dc excited glow discharges in atmospheric pressure air in pin-to-water electrode systems. *J. Phys. D: Appl. Phys.* **41**, 215201 (2008).
19. Staack, D., Farouk, B., Gutsol, A. F. & Fridman, A. Spatially resolved temperature measurements of atmospheric-pressure normal glow microplasmas in air. *IEEE Trans. Plasma Sci.* **35**, 1448–1455 (2007).
20. Mezei, P., Cserfalvi, T. & Janossy, M. On the pressure dependence of the positive column cross section in high-pressure glow discharges. *J. Phys. D: Appl. Phys.* **34**, 1914–1918 (2001).
21. Marcus, R. K. & Broekaert, J. A. C. *Glow discharge plasmas in analytical spectroscopy*. (John Wiley and Sons, Chichester, West Sussex, England, UK, 2003).
22. Wang, Y. Q., Chong, N., Dong, L. M., Tang, Y. J. & Song, H. J. Study on electronic excitation temperature of argon plasma using low pressure micro-ICP excitation source. *Adv. Mater. Res.* **383**, 1844–1848 (2012).
23. Lu, X., Jiang, Z., Xiong, Q., Tang, Z. & Pan, Y. A single electrode room-temperature plasma jet device for biomedical applications. *Appl. Phys. Lett.* **92**, 151504 (2008).
24. Xian, Y., Lu, X., Tang, Z., Xiong, Q., Gong, W., Liu, D., Jiang, Z. & Pan Y. Optical and electrical diagnostics of an atmospheric pressure room temperature plasma plume. *J. Appl. Phys.* **107**, 063308 (2010).
25. Xiong, Q., Nikiforov, A. Y., Lu, X. P. & Leys, C. High-speed dispersed photographing of an open-air argon plasma plume by a grating–ICCD camera system. *J. Phys. D: Appl. Phys.* **43**, 415201(2010).
26. Pekárek, S. DC corona discharge ozone production enhanced by magnetic field. *Eur. Phys. J. D* **56**, 91–98 (2010).
27. Richards, A. D., Thompson, B. E. & Sawin, H. H. Continuum modeling of argon radio frequency glow discharges. *Appl. Phys. Lett.* **50**, 492–494 (1987).
28. Jiang, W., Tang, J., Wang, Y., Zhao, W. & Duan, Y. A low-power magnetic-field-assisted plasma jet generated by dielectric-barrier discharge enhanced direct-current glow discharge at atmospheric pressure. *Appl. Phys. Lett.* **104**, 013505 (2014).
29. Lifshitz, A. Correlation of vibrational de-excitation constant (k0-1) of diatom molecules. *J. Chem. Phys.* **61**, 2478–2479 (1974).

Acknowledgments

This work was financially supported by the CAS/SAFEA International Partnership Program for Creative Research Teams and the China Postdoctoral Science Foundation under Grant No. 2012M512041.

Author contributions

W.Z. and J.T. led the project and supervised all the experiments. W.J. and J.T. conducted experiments and measurements and fulfilled data analysis and physical interpretations. J.T., W.J., Y.W., W.Z. and Y.D. discussed the results. W.J. and J.T. co-wrote the manuscript.

Additional information

Competing financial interests: The authors declare no competing financial interests.

How to cite this article: Jiang, W., Tang, J., Wang, Y., Zhao, W. & Duan, Y. Characterization of argon direct-current glow discharge with a longitudinal electric field applied at ambient air. *Sci. Rep.* **4**, 6323; DOI:10.1038/srep06323 (2014).